Fundamental Limits on Subwavelength Range Resolution

Andrew N. Jordan[1,2,*] and John C. Howell[1,3]

[1]*Institute for Quantum Studies, Chapman University, Orange, California 92866, USA*

[2]*Department of Physics and Astronomy, University of Rochester, Rochester, New York 14627, USA*

[3]*Racah Institute of Physics, The Hebrew University of Jerusalem, Jerusalem 91904, Israel*

We establish fundamental bounds on subwavelength resolution for the radar ranging problem, "super-radar." Information-theoretical metrics are applied to probe the resolution limits for the case of both direct electric field measurement and photon-counting measurements. To establish fundamental limits, we begin with the simplest case of range resolution of two point targets from a metrology perspective. These information-based metrics establish fundamental bounds on both the minimal discrimination distance of two targets and the precision on the separation of two subwavelength resolved targets. For the minimal separation distance, both the direct field method and photon counting method show that the discriminability vanishes quadratically as the target separation goes to zero, and is proportional to the variance of the second derivative of the electromagnetic field profile. Nevertheless, robust subwavelength estimation is possible. Several different band-limited function classes are introduced to optimize discrimination. We discuss the application of maximum likelihood estimation to improve the range precision with optimal performance. The general theory of multiparameter estimation is analyzed, and a simple example of estimating both the separation and relative strength of the two point reflectors is presented.

I. INTRODUCTION

Radar and lidar are powerful remote sensing techniques used in a wide array of applications, such as archaeology, utilities, navigation, topographical mapping, distance and velocity detection, civilian air traffic control, and tracking and detection of satellites and spacecraft [1–8]. Range resolution in radar [6,9,10] or lidar [11–13] is the smallest measurable distance between two objects within the same angular direction. Range resolution is vital in target characterization and imaging. For decades, disambiguation of the two objects was determined solely by temporally resolving the pulses which reflected from each of the objects; see, for example, [6,14]. When the range resolution distance d_r obeys the inequality $d_r \geq c\tau/2$, where c is the speed of light, τ is the pulse width and 2 comes from the round trip of the pulse [9,10,15], the two objects are considered resolved.

Recently, the authors showed that the coherent interference created from the pulses reflecting from the objects could be used to greatly improve upon existing definitions of range resolution [16]. When two identical, but slightly shifted in time, radar or coherent lidar pulses are summed,

they create a new composite pulse. The novel interference technique employed by the authors relied on a self-referential signal that compared the resulting interference feature in a region of steep gradients with a zero gradient portion of the signal. Single parameter estimation allowed for precise determination of small relative shifts between two component pulses achieving far superior resolution than the inverse bandwidth can achieve.

The critical insight is to use an amplitude-based resolution paradigm together with parameter estimation, rather than a temporally resolved paradigm. The self-referencing nature of the estimation using only relative amplitudes within the returning pulse, rather than absolute amplitude, permits us to distinguish target properties from loss. We assume here that the character of the pulse shape is preserved by the intermediate medium. In general, a frequency-dependent index of refraction will cause pulse distortion that will need to be accounted for in realistic applications. However, in establishing fundamental bounds, we focus on the simplest case of an undistorted pulse shape.

We note that this work is fundamentally different than parameter estimation applied to incoherent imaging. The latter permits the estimation of the distance between two point sources better than the Rayleigh criterion using mode sorting of spatial optical modes (see, for example, [17–20]), which can be extended to multiparameter estimation

---

*jordan@chapman.edu

064046-1

[21,22]. We detail why these two methods are completely different. First, in the imaging case, the method is constrained to solving the problem for a given point-spread function of the imaging system. For our case, we can use arbitrary input pulses. We expect that this freedom will be instrumental in scattering reconstruction for complex objects. Second, the point sources in the imaging problem are usually incoherent. Our system is fully coherent, allowing for interference between the returning waves from the various scatterers. Third, imaging superresolution relies on spatial mode decomposition where our method uses the direct measurement of the full waveform for radio wave or photon detection arrival times.

In the previous work [16], we used a balanced self-referencing estimation method to compare ratios of differences of the measured function at different space (or time) points to define a signal that was used to infer the distance between the two objects. While the basic features of the super-radar functions were outlined and demonstrated in our previous paper, only minimal discussion of noise was presented. Here we more formally address fundamental range resolution bounds using information-theoretical metrics. We give treatments of direct measurement of electric fields of pulses of electromagnetic radiation, which is most suitable for radar applications, as well as in the photon-counting case, which is especially useful for coherent lidar. An important concept for the noise models we describe is the Fisher information of the separation parameter. This information metric sets a bound on the smallest variance of the parameter for large data sets over all estimators in the large data set limit, which sets the fundamental bound of our method. We also find that the overlap between waveforms of different separations as well as the QFI are useful and give additional insight into the parameter estimation. We discuss different estimators, including maximum likelihood as well as Bayesian estimation methods. We end with a discussion of the generalization to multiparameter estimation, which will be critical to making this technique useful in realistic applications. We stress that this work employs Fisher information techniques to address fundamental range resolution (i.e., resolving two objects) limits and not ranging accuracy limits (i.e., determining the distance to a target) as has been done by others [23–25].

The paper is organized as follows. In Sec. II we introduce the basic concepts of the remote sensing range resolution task. In Sec. III we consider direct electric field detection, as appropriate for radio or microwave frequency electromagnetic radiation and radar applications. There we compute the Fisher information of the target distance, which sets the best-case precision of range resolution, relative to the returning signal amplitude to detector noise ratio. In Sec. IV we consider a photon-counting detector as appropriate for optical frequencies and lidar applications, and consider three different information-theoretical metrics: a wave overlap metric to distinguish different

values of the unknown parameter; the classical Fisher information for spatially (or temporally) resolved photon detection; and the QFI metric, where the measured basis is optimized to extract maximal information about the parameter. In Sec. V we discuss different kinds of waveforms that are able to resolve subwavelength structure using this technique. We discuss band-limited pulses, a line-segment triangle wave, and frequency combs. Generalizations to multiparameter estimation, as derived in Sec. VI, and a two-parameter example are discussed consisting of range resolution and relative reflection strength. Section VII concludes.

II. RANGE RESOLUTION IN REMOTE SENSING

We consider the simplest case of two equal-amplitude point scatterers of electromagnetic radiation, and our task is to determine the minimal discrimination distance of the two targets and the precision on the range between them, focusing on subwavelength range resolution. We introduce a simple one- dimensional model, where the electric field has a spatial envelope of the form $f(x)$ which is sent out, and a return wave of the form

$$f_l(x) = \frac{1}{2}(f(x - l/2) + f(x + l/2)), \tag{1}$$

is detected. For simplicity, we have chosen to set the origin halfway between the two scattering centers. Here l is the distance between the two scatterers that we wish to estimate. In a remote sensing context, the amplitude of the returning pulse is typically attenuated from the outgoing intensity by many orders of magnitude, so the absolute amplitude of the pulse is assumed to be unrelated to the target properties, and cannot not be used in the estimation task. Consequently, we must consider the *normalized state* [Eq. (1)] and consider either the amplitude of the returning field relative to the detector noise, or the number of *detected* photons as the metrological resource. In the sections below we assume the function f is analytic and normalized. We are most interested in the case where the function is *band-limited*, having an upper frequency cutoff Ω, and when the range resolution parameter $l < 2\pi/\Omega$, breaking the long-standing tradeoff between target resolution and wave carrier frequency. We note that we have set the velocity of the pulse inside the medium equal to unity.

III. FIELD DETECTION

In this section we focus on the detection of the electric field of the radiation via the use of amplifiers. We consider primarily radio frequencies in this section for radar applications. In this frequency range, direct detection of the field is possible via amplification of the detected electromagnetic signals, leading to noise added to the signal waveform that is related to the effective amplifier temperature. Here we consider a model to determine the ultimate

limits of the precision on the distance between two scattering centers. Let the detected signal from the amplifier be $s(t)$, and we time-discretize in units of the time resolution of the detector Δt. We convert to an effective distance x to connect to the above discussion via the propagation speed of the wave and add a noise term arising from the amplifier,

$$s_i = \mathcal{N}_l f_l(x_i) + \sigma \xi(x_i), \tag{2}$$

where the signal has been rescaled so that the overlap signal is normalized with the normalization factor $\mathcal{N}_l$, which is l-dependent. Since the noise power of the amplified signal is known from the detector properties, the total signal can be scaled appropriately to normalize it. The normalization condition yields the following expression for $\mathcal{N}_l$:

$$\mathcal{N}_l^2 = \frac{2}{1 + \int_{-\infty}^{\infty} dx f(x + l/2) f(x - l/2)}. \tag{3}$$

Clearly $\mathcal{N}_l \to 1$ as $l \to 0$ because we choose $f(x)$ to be normalized. The detected signal s_i contains σ which is the noise strength, Δx which is the converted discretized space unit (using the wave speed) and $\xi(x_i)$ which is a unit strength, white noise random variable with correlation

$$\langle \xi(x_i)\xi(x_j)\rangle = \delta_{ij}. \tag{4}$$

In a remote detection setup, the returning signal strength is unknown, so we keep the signal normalized, and thus the noise level σ of the detector will also be rescaled depending on the signal strength.

We can pen a probability model for the above signal-plus-noise point of view as

$$P(\{s_i\}|l) = \prod_i \frac{1}{\sqrt{2\pi\sigma^2}} \exp\left(-\frac{(s_i - \mathcal{N}_l f_l(x_i))^2}{2\sigma^2}\right), \tag{5}$$

where $P_l(\{s_i\}|l)$ is the probability density of the sequence of signal data points s_i, given the value of the parameter l. The Fisher information [26] about the parameter l in the above distribution is defined as

$$I(l) = \prod_i \int_{-\infty}^{\infty} \left(\frac{\partial \ln P_l(s_i)}{\partial l}\right)^2 P_l(s_i) ds_i$$
$$= -\prod_i \int_{-\infty}^{\infty} \left(\frac{\partial^2 \ln P_l(s_i)}{\partial l^2}\right) P_l(s_i) ds_i. \tag{6}$$

Here $P_l(s_i)$ is the probability of a single data point given a fixed l. The inverse Fisher information bounds the variance of any unbiased estimator $\hat{l}$ of the parameter l, for large data

sets

$$\mathrm{Var}[\hat{l}] \geq \frac{M}{I(l)}, \tag{7}$$

where M is the number of repetitions of the measurement, the Cramér-Rao bound [27]. The Fisher information formalism has been widely applied to bound estimation precision in coherent optics; see, for example, [28].

For the super-radar ranging problem, the logarithm of the distribution turns the product into a sum, so the resulting field-detection Fisher information for $M = 1$ is given by

$$I_f = \frac{1}{\sigma^2} \sum_i \left(\frac{\partial(\mathcal{N}_l f_l(x_i))}{\partial l}\right)^2. \tag{8}$$

In white noise models, the total noise power grows as $\int dx_1 dx_2 \langle \Delta s(x_1) \Delta s(x_1)\rangle = \int dx \sigma^2 = \sigma^2 X = \sigma^2 \Delta x N$, where N is the number of data points. Thus, we can account for making the time bins (converted here to space bins) wider by defining the noise density $\Sigma^2 = \sigma^2 \Delta x$, so we can turn the sum into an integral to approximate the Fisher information as

$$I_f \approx \frac{1}{\Sigma^2} \int dx \left(\frac{\partial(\mathcal{N}_l f_l(x))}{\partial l}\right)^2. \tag{9}$$

This result can be further simplified for the range resolution problem as

$$\Sigma^2 I_f = -(\partial_l \ln \mathcal{N}_l)^2 + \frac{\mathcal{N}_l^2}{16} \int dx (f'(x + l/2)$$
$$- f'(x - l/2))^2. \tag{10}$$

The small l behavior can be found by expanding all terms to leading order in l. The zeroth- and first-order terms vanish, leaving the quadratic approximation near $l = 0$,

$$\Sigma^2 I_f \approx \frac{l^2}{16}\left(\int dx f''(x)^2 - \left(\int dx f'(x)^2\right)^2\right) + \mathcal{O}(l^3). \tag{11}$$

Here we assume well-defined first and second derivatives of the function $f(x)$, as well as square integrability.

As we will explore later on in the paper, let us define the f-dependent quantity in the large parentheses as $\mathrm{var}[d^2]_f$, a measure of the variance of the second derivative of f, which is a measure of the variation of the function f over its range in space (or time). If we define $\delta[d^2]_f = \sqrt{\mathrm{var}[d^2]_f}$ as its standard deviation, then we can bound

the relative error $\delta l/l$ of the range resolution l in the deep subwavelength limit from (7) as

$$\frac{\delta l}{l} \geq \frac{4\Sigma}{\sqrt{M} l^2 \delta[d^2]_f}. \qquad (12)$$

This is a main result of this paper. We note that when $\delta[d^2]_f$ is comparable to Ω^2, the band limit of the pulse, implying $l^2 \delta[d^2]_f < 1$, then by having many data sets with good signal-to-noise ratio (i.e., $\sqrt{M}/\Sigma \gg 1$), relative errors less than 1 are easily achieved. Compared with the traditional criterion for range-resolved targets, where l must be larger than the pulse width, our bound inequality (12) can beat this criterion by many orders of magnitude.

A. Estimators

We can implement several different estimators. We first consider *maximum likelihood estimation* (or MaxLike for short). We define the log-likelihood function $\mathcal{L}(l)$ as the natural logarithm of the probability of obtaining the sequence $\{s_i\}$ of measurement outcomes given the value of the unknown parameter is l. MaxLike is defined as assigning an estimator $\hat{l}_{\mathrm{ml}}$ such that

$$\hat{l}_{\mathrm{ml}} = \mathrm{argmax}[\mathcal{L}(l)]. \qquad (13)$$

Here argmax is the value taken at the maximization of the log-likelihood function. For our problem [Eq. (5)] the log-likelihood function is given by

$$\mathcal{L} = -\sum_j \frac{(s_j - \mathcal{N}_l f_l(x_j))^2}{2\sigma^2} + \mathrm{const}. \qquad (14)$$

If there are M repetitions of the measurement for each x value then the data is indexed as $s_j^{(k)}$, where k ranges from 1 to M, and the sum in $\mathcal{L}$ is over both j and k. The MaxLike condition given the data set $\{s_j^{(k)}\}$, for the estimated value of l, is given by the condition

$$\partial_l \sum_{j,k} s_j^{(k)} \mathcal{N}_l f_l(x_j) = 0, \qquad (15)$$

where we used the fact that the function is normalized at this signal-to-noise level. The above simple result is very appealing: in practice, one can define two vectors $\mathbf{u}, \mathbf{v}$ of size N with elements consisting of the measured data for the first vector $u_j = s_j$, and the second is a series of trial vectors defined by elements $v_j = \mathcal{N}_l f_l(x_j)$ for a variety of different values of l. The first vector can carry out the sum the data $u_j \rightarrow \sum_{k=1}^M s_j^{(k)}$ for different values of M to gain improved accuracy. Accuracy is improved because the signal grows as M but the noise only grows as $\sqrt{M}$. The dot

product between the two vectors $\mathbf{u} \cdot \mathbf{v}$ is then plotted versus the different trial values of l. When the dot product reaches its maximum, that is the MaxLike estimated value for l.

There is an intuitive reason why the above procedure is optimal. Let us recall the starting point of this analysis, Eq. (2). Let l_t be the true value of l that is sampled with the data, and let l be the trial value that will be scanned. We can write the function to be maximized as

$$\sum_j s_j \mathcal{N}_l f_l(x_j) \approx \int dx [\mathcal{N}_{l_t} f_{l_t}(x) + \xi(x)] \mathcal{N}_l f_l(x). \qquad (16)$$

When integrating over the random variable, that term tends to be zero, while the first term is simply the overlap between two normalized vectors,

$$\langle f_{l_t} | f_l \rangle = \mathcal{N}_{l_t} \mathcal{N}_l \int dx f_{l_t}(x) f_l(x), \qquad (17)$$

where we introduced Dirac notation for the inner product of the two normalized waves. The overlap can be at most 1 when the value $l = l_t$, which is where the maximum value is reached. Any other value of l must necessarily lead to an overlap less than 1. From this point of view, we see that even if the rescaling is not perfectly normalized, the log-likelihood function will still be maximized at the true value of l.

Indeed, we can go further and approximate the log-likelihood function, Eq. (14), in the vicinity of the true value of l by writing $\mathcal{N}_l f_l(x) \approx \mathcal{N}_{l_t} f_{l_t}(x) + \partial_l(\mathcal{N}_l f_l(x))(l - l_t)$ and taking an average over the fluctuations to find

$$\mathcal{L} \approx \mathrm{const} - \frac{M}{2\Sigma^2} \int dx (\partial_l \mathcal{N}_{l_t} f_{l_t}(x))^2 (l - l_t)^2. \qquad (18)$$

Therefore, the uncertainty of the MaxLike method is set by the width of the log-likelihood curve in the large data limit,

$$\langle \mathcal{L}(l) \rangle = \mathrm{const} - \frac{(l - l_t)^2}{2\sigma_{\mathrm{ml}}^2}, \qquad (19)$$

where the statistical uncertainty on l is given by σ_{ml}, which is Gaussian in the large data limit by the central limit theorem. The variance is given by the inverse Fisher information,

$$\sigma_{\mathrm{ml}}^2 = \frac{1}{M I_f(l)}. \qquad (20)$$

Without averaging, the log-likelihood is given for a single realization of the data processing as

$$\mathcal{L}(l) = \mathrm{const} - \frac{(l - \hat{l}_{\mathrm{ml}})^2}{2\sigma_{\mathrm{ml},1}^2}, \qquad (21)$$

where $\sigma_{\mathrm{ml},1}^2$ is the $M = 1$ variance. The statistic $\hat{l}_{\mathrm{ml}}$ can be found by fitting data to a parabola, and further averaging over M repetitions to improve precision. If $\hat{l}_{\mathrm{ml},j}$ is the

MaxLike estimator for the jth trial of the M repetitions, then the variance $(1/M) \sum_j (\hat{l}_{\mathrm{ml},j} - \langle \hat{l}_{\mathrm{ml}} \rangle)^2$ is given by

$$\mathrm{Var}[\hat{l}_{\mathrm{ml}}] = \frac{\mathrm{Var}[\hat{l}_{\mathrm{ml},1}]}{M} \geq \frac{1}{M I_{f,1}}, \qquad (22)$$

where $I_{f,1}$ is the one-trial Fisher information. We assume each trial is independent of the others. Formal proofs of the results above may be found in the statistics literature [26,29,30] and arise from the central limit theorem.

Another estimation technique is *Bayesian estimation*. In this method a probability distribution is given to l that quantifies our degree of belief about the value of l. The prior distribution is defined as $P_0(l)$. The likelihood is the probability distribution of the data, given an assumed (and fixed) value of l. We now use Bayes' theorem to find the probability of the value l, given a set of data taken from the above model,

$$P(l|\{s_j\}) = \frac{P(\{s_j\}|l) P_0(l)}{P(\{s_j\})}, \qquad (23)$$

where $P(\{s_j\}) = \int dl P(\{s_j\}|l) P_0(l)$. The new probability distribution $P(l|\{s_j\})$ is the posterior distribution for l, given the data collected. If the posterior distribution is maximized, then we see the Bayesian estimator can be shifted away from the MaxLike estimator based on prior knowledge. However, if a uniform prior is chosen, then the maximum of the distribution coincides with the Max-Like estimator. A more refined Bayesian estimator is given by the average of l in the posterior distribution, and the variance of the estimator can be computed as the variance of l in the posterior distribution. This procedure is generally more resource intensive because an entire distribution needs to be calculated for each value of l. While a uniform prior is common and leads to the MaxLike estimator, it may be advantageous to choose the Jeffreys prior because the Fisher information vanishes at $l = 0$,

$$P_0(l) = \frac{\sqrt{I_f(l)}}{n}, \quad n = \int dl \sqrt{I_f(l)}. \qquad (24)$$

For this choice, $P_0(l)$ vanishes linearly near the origin as $P_0(l) \sim (l/4)\delta(d^2)$, where $\delta(d^2)$ is the standard deviation of the second derivative.

IV. PHOTON DETECTION

In this section we consider the complementary problem of using direct photon detection of radiation returning from a target. This analysis is suitable for lidar applications. The photons are assumed to be time-resolved and tagged with their arrival time t_i. In the analysis below, we convert this to a position label x_i with the wave speed. We will consider three different estimation approaches to determine

the range parameter l: an inner product metric (overlap criterion); the Fisher information of the time-resolved photodetected events; and, finally, the QFI, which optimizes over all possible choices of measurement basis.

A. Overlap metric: state distinguishability

The ability to distinguish the original waveform (with $l = 0$) from a returned signal with nonzero l can be quantified with the overlap of the two waveforms. Perfect distinguishability is obtained when the overlap is zero, but statistical discrimination for the hypothesis testing is possible when the overlap is less than 1; see, for example, [31]. Let us define the overlap between the return signal and the outgoing signal (here we assume both are normalized, with $\mathcal{N}_l$ being the normalization of $|f_l\rangle$) as

$$\langle f | f_l \rangle = \mathcal{N}_l \int_{-\infty}^{\infty} dx f(x)^* f_l(x) \qquad (25)$$

$$= \mathcal{N}_l \int_{-\infty}^{\infty} dx f(x - l/4) f(x + l/4). \qquad (26)$$

Here we symmetrized and combined the two terms, taking f real for simplicity. We note that this overlap is a special case of Eq. (17), focusing on the case where the task is to disseminate the separation distance of l from the null hypothesis that there is no separation.

We can expand in powers of l (assuming a differentiable function) and integrate by parts to find that while both the normalization and the overlap integral have an order l^2 term in the product that cancel out, leaving an order l^4 term as the leading-order behavior,

$$\mathcal{N}_l = 1 + \frac{l^2}{8} \int_{-\infty}^{\infty} f'^2 dx + \frac{l^4}{32} \left(\frac{3}{4} \left(\int_{-\infty}^{\infty} f'^2 dx \right)^2 \right.$$
$$\left. - \frac{1}{3} \int_{-\infty}^{\infty} dx f^{(4)} f \right) + \dots, \qquad (27)$$

while

$$\int_{-\infty}^{\infty} dx f\left(x - \frac{l}{4}\right) f\left(x + \frac{l}{4}\right)$$
$$= 1 - \frac{l^2}{8} \int_{-\infty}^{\infty} f'^2 dx + \frac{l^4}{384} \int_{-\infty}^{\infty} dx f^{(4)} f + \dots, \qquad (28)$$

so the combined expansion is given by

$$\langle f | f_l \rangle = 1 - \frac{l^4}{128} \left(\int_{-\infty}^{\infty} dx f^{(4)} f - \left(\int_{-\infty}^{\infty} f'^2 dx \right)^2 \right)$$
$$+ \dots. \qquad (29)$$

Thus, in order to maximize distinguishability, we should minimize the above expression. This is clearly in the special case where l is small on the scale of the features of $f(x)$.

B. Fisher information for position measurements

We now investigate the Fisher information metric. We assume the system is measured in a time-resolved manner, which we convert to a position basis via the wave speed. The Fisher information about the parameter l for photon detection is defined for probability distributions $p_l(x)$ as

$$I_p = \int_{-\infty}^{\infty} \left(\frac{\partial \ln p_l(x)}{\partial l} \right)^2 p_l(x) dx \tag{30}$$

$$= -\int_{-\infty}^{\infty} \left(\frac{\partial^2 \ln p_l(x)}{\partial l^2} \right) p_l(x) dx. \tag{31}$$

We can simplify this formula if we consider the square of the photon state as our probability distribution

$$p_l(x) = \mathcal{N}_l^2 |f_l(x)|^2. \tag{32}$$

Here we have renormalized the distribution with a prefactor $\mathcal{N}_l$, such that the distribution $p_l(x)$ is normalized for all l.

An important aspect of the radar ranging problem is that, in remote sensing, the amount of radiation received from the target is typically many orders of magnitude reduced in intensity. Therefore, the total Fisher information is the normalized probability of return times the total number of photons in the return signal. Inserting this formula for the radar ranging problem, we find the result $I_p = I_1 + I_2$, where

$$I_1 = \frac{\mathcal{N}_l^2}{4} \int_{-\infty}^{\infty} dx \left(f'(x - l/2)^2 + f'(x + l/2)^2 \right)$$

$$= \frac{\mathcal{N}_l^2}{2} \int_{-\infty}^{\infty} dx f'(x)^2, \tag{33}$$

in which the prime denotes an x derivative and in the second equality we shifted the integration variable, and

$$I_2 = -\frac{\partial^2}{\partial l^2} \ln \mathcal{N}_l^2. \tag{34}$$

We observe that the only l-dependence in the Fisher information occurs in the normalization of the function. Despite the different-looking expressions for the photon-detection Fisher information I_p of Eqs. (33) and (34) and the field Fisher information [Eq. (10)], they are in fact equivalent up to a factor of 4, that is, $4\Sigma^2 I_f = I_p$.

The leading-order behavior for small l is given by expanding both I_1 and I_2 to second order in l to find

$$I_2 = -\frac{1}{2} \int_{-\infty}^{\infty} dx f'^2 + \frac{l^2}{2} \left(-\frac{3}{4} \left(\int_{-\infty}^{\infty} dx f'^2 \right)^2 \right.$$

$$\left. + \frac{1}{2} \int_{-\infty}^{\infty} dx f^{(4)} f \right) + \mathcal{O}(l^4), \tag{35}$$

where the (4) indicates the fourth-order derivative with respect to x, and

$$I_1 = \frac{1}{2} \int_{-\infty}^{\infty} dx f'^2 + \frac{l^2}{8} \left(\int_{-\infty}^{\infty} dx f'^2 \right)^2 + \mathcal{O}(l^4). \tag{36}$$

Putting these results together to find the total Fisher information, we see that the zeroth order in l term vanishes, leaving only the second-order term, $I_{\text{tot}} = I_1 + I_2$,

$$I_{\text{tot}} \approx \frac{l^2}{4} \left(\int_{-\infty}^{\infty} dx f^{(4)} f - \left(\int_{-\infty}^{\infty} dx f'^2 \right)^2 \right), \tag{37}$$

with a fourth-order correction in l. Thus, at $l = 0$, there is no Fisher information to be had, and we need to go to the second-order term in l for small l. We notice that the result to this order can be expressed in terms of the variance of an operator $\hat{O} = -d^2/dx^2$ in the state f. Indeed, we will see this more explicitly in the next subsection.

C. Quantum Fisher information metric

We now investigate the quantum Fisher information (QFI) metric. The QFI permits the further optimization of the parameter over all possible choices of measurement basis [32,33]. The QFI about the parameter l is defined for pure states as

$$F = 4(\langle \partial_l f_l | \partial_l f_l \rangle - |\langle \partial_l f_l | f_l \rangle|^2). \tag{38}$$

The QFI metric gives a lower bound for the variance of any unbiased estimator $\tilde{l}$ of the parameter l,

$$\text{Var}[\tilde{l}] \geq \frac{M}{F}, \tag{39}$$

where M is the number of measurements taken, which we consider to be the number of detected photons. Thus, we wish to maximize the information acquired about the parameter l in order to minimize the statistical uncertainty.

From a quantum-mechanical perspective, we can write the radar ranging state $f_l(x)$ as

$$|f_l\rangle = \mathcal{N}_l(e^{-il\hat{p}/2}|f\rangle + e^{il\hat{p}/2}|f\rangle)/2, \tag{40}$$

where $\hat{p} = -i\partial_x$ is the momentum operator, so its exponential shifts the original state f by an amount $\pm l/2$.

Here we normalized the state from the start. Thus, the shifted state can therefore be written as

$$|f_l\rangle = \mathcal{N}_l \cos(l\hat{p}/2)|f\rangle. \tag{41}$$

The normalization can be found explicitly:

$$\mathcal{N}_l^2 = \frac{1}{\langle f \mid \cos^2(l\hat{p}/2)|f\rangle}. \tag{42}$$

We note that the l-derivative is given by

$$|\partial_l f_l\rangle = -\frac{\hat{p}}{2}\sin(l\hat{p}/2)|f\rangle + \mathcal{N}_l'\cos(l\hat{p}/2)|f\rangle. \tag{43}$$

Inserting these results into the expression for the QFI, we find the second term in Eq. (38) is zero, while the first may be written as

$$F = 4\left(\frac{\langle f|\hat{A}^2|f\rangle\langle f|\hat{B}^2|f\rangle - \langle f|\hat{A}\hat{B}|f\rangle^2}{\langle f|\hat{B}^2|f\rangle^2}\right), \tag{44}$$

where we define the operators

$$\hat{A} = \frac{\hat{p}}{2}\sin(l\hat{p}/2), \quad \hat{B} = \cos(l\hat{p}/2). \tag{45}$$

This is a general result for the radar ranging problem with two equal-weight point scatterers. We note that by the Cauchy-Schwarz inequality for operators, the QFI F must be positive. This statement can be proved by considering the expectation value of the square of the operator $\langle f|\hat{B}^2|f\rangle\hat{A} - \langle f|\hat{A}\hat{B}|f\rangle\hat{B}$, in the state $|f\rangle$, which must be positive.

We now focus on the special case where l is small compared to the typical inverse momentum component of f, to obtain the leading-order expression in l:

$$F = \frac{l^2}{4}\text{Var}\left[\hat{p}^2\right]_f + \mathcal{O}(l^4), \tag{46}$$

where we defined the variance of the operator in the state f as $\text{Var}[\cdot]_f$. We see immediately that in the position basis, we recover our previous result for the classical Fisher information, as is expected.

The variance can be calculated most easily in momentum space (k) to find

$$\text{Var}\left[\hat{p}^2\right]_f = \int_{-\infty}^{\infty} dk|\tilde{f}(k)|^2 k^4 - \left(\int_{-\infty}^{\infty} dk|\tilde{f}(k)|^2 k^2\right)^2, \tag{47}$$

where $\tilde{f}$ is the Fourier transform of f.

V. SUBWAVELENGTH RESOLVING STATES

We now explore different states that could maximize the Fisher information.

A. Sinc derivatives

We first consider the class of band-limited functions

$$g_n(x) = N_n \frac{d^n}{dx^n}\text{sinc}(k_0 x), \tag{48}$$

where N_n is the normalization of the function and k_0 is the band limit we consider. We consider n even. In this case, the functions are even, so we can write the overlap as a convolution $g_n \star g_n(-l/2)$. Using the convolution theorem, we can write the Fourier transform on the variable $l/2$ as

$$\int_{\infty}^{\infty} d(l/2)\langle g|g_n\rangle e^{ikl/2} = |\tilde{g}_n(k)|^2, \tag{49}$$

where $\tilde{g}_n(k)$ is the Fourier transform. In this case, the Fourier transform of the nth derivative of the sinc function is quite simple:

$$\tilde{g}_n(k) = (ik)^n \text{Box}[k - k_0], \tag{50}$$

where the Box function is 1 for $-k_0 < k < k_0$ and 0 elsewhere.

We can calculate the variance [Eq. (47)] for the class of function g_n discussed above. We find

$$\langle\hat{p}^2\rangle = \frac{2n+1}{2n+3}k_0^2, \quad \langle\hat{p}^4\rangle = \frac{2n+1}{2n+5}k_0^4. \tag{51}$$

Thus, the variance of $\hat{p}^2$ is given by

$$\text{Var}[\hat{p}^2] = k_0^4 \frac{4(2n+1)}{(2n+5)(2n+3)^2}. \tag{52}$$

However, the Fisher information about l vanishes in the large n limit, so these functions are not helpful despite being band-limited.

B. Frequency combs

We consider now delta-function peaks in the frequency space. The simplest such combination is a monochromatic tone. We consider the case often encountered in metrology of

$$|\tilde{f}(k)|^2 = [\delta(k - k_0) + \delta(k + k_0)]/2. \tag{53}$$

This function gives a monochromatic tone with frequency k_0, say $\sin(k_0 x)$. Unfortunately, while this function has good variance of $\hat{p}^2$, it has exactly zero variance of $\hat{p}^4$, so

there is no information about the l parameter. This fact is clear from working in the original position (or time) space, where Eq. (1) is given by

$$[\sin(k_0(x - l/2)) + \sin(k_0(x + l/2))]/2$$
$$= \sin(k_0 x)\cos(k_0 l/2), \tag{54}$$

so after normalization of the function, there is no l information for any value of l.

However, it is not difficult to create a variance of $\hat{p}^2$: we add in a dc offset at $k = 0$, so that all are equally weighted,

$$|\tilde{f}(k)|^2 = [\delta(k - k_0) + \delta(k) + \delta(k + k_0)]/3. \tag{55}$$

Then the variance is given by

$$\text{Var}[\hat{p}^2] = \frac{2k_0^4}{9}. \tag{56}$$

More generally, we can consider a set of discrete frequencies k_j, with weights c_j^2, resulting in

$$\langle\hat{p}^2\rangle = \sum_j k_j^2 c_j^2, \quad \langle\hat{p}^4\rangle = \sum_j k_j^4 c_j^2. \tag{57}$$

For the case of a comb of N regularly spaced frequencies $k_j = jk_0$ of weights c_j^2, we have

$$|\tilde{f}(k)|^2 = \sum_{j=-N}^{N} c_j^2 \delta(k - jk_0). \tag{58}$$

If we take the $2N + 1$ states to have the same weight $1/(2N + 1)$, then we find the result

$$\text{Var}[\hat{p}^2] = \frac{k_0^4 N(N + 1)(4N^2 + 4N - 3)}{45} \approx \frac{4k_{\max}^4}{45}, \tag{59}$$

where we denoted the highest frequency appearing as $k_{\max} = Nk_0$.

C. Bandlimited pulse

We follow our earlier article [16] and consider our interference class function to be a product of two functions, $f(x) = c_m(x)f_n(x)$, where c_m is the "canvas" function, and f_n is an approximation of the function we are interested in creating a band-limited version of [34]. Beyond setting the band limits, the canvas function also enforces square integrability of $f(x)$ if chosen to decay sufficiently faster than the divergence of the polynomial $f_n(x)$, so we restrict to the case $m > n$. We use the Ω-band-limited canvas functions

$$c_m(x) = \text{sinc}\left(\frac{\Omega x}{m}\right)^m \tag{60}$$

where m governs the power of decay. The Fourier transform of $c_m(x)$ is strictly zero above frequency Ω. The polynomial $f_n(x)$ is defined as

$$f_n(x) = \sum_{k=0}^{n-1} a_k x^k, \tag{61}$$

where the a_k are chosen to be the Taylor coefficients of the desired function f up to order $n - 1$. We use the polynomial function

$$f_n(x) = 8x - 14.3984x^3 + 4.77612x^5 - 0.82315x^7, \tag{62}$$

along with the $c_{10}(x)$ canvas function with scaled dimensionless bandwidth $\Omega = 2\pi$. A new method of creating band-limited functions that closely approximate a desired function in a finite region was recently introduced [35]. The function $f(x)$ has steep regions as well as flat regions
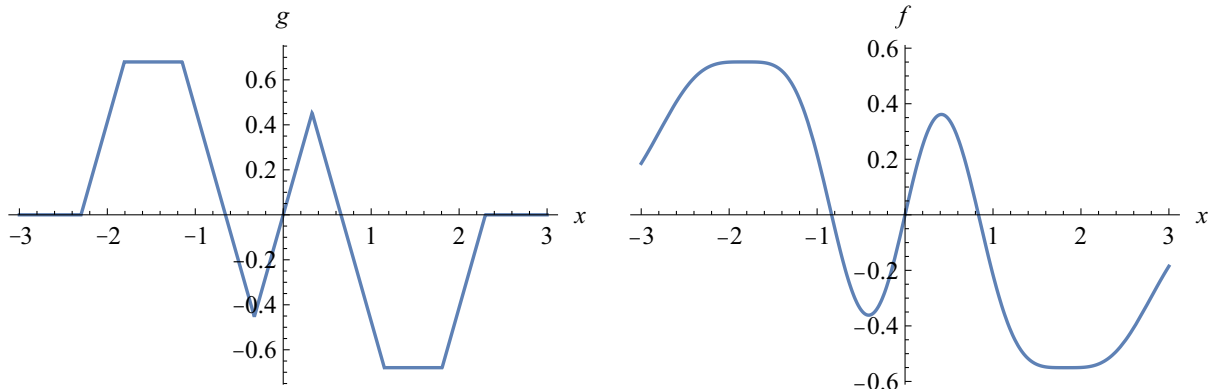

FIG. 1. Two waveforms for super range resolution. The function f is band-limited (see text), while the function $g(x)$ (left) is a line-segment "triangle" function that mimics it with segments of either steep slope or zero slope. The triangle function is chosen so that it has equal slopes and equal intervals. Both functions are normalized and the slope of the triangle function g chosen to match the slope of the band-limited function f at $x = 0$.

to easily distinguish reflector range from loss, as shown in the right panel of Fig. 1 (we set the wave speed to 1). A line segment function ("triangle function") that captures the main features is shown in the left panel. Both functions are normalized and the slope of the triangle function is matched to the slope of the band-limited function at $x = 0$.

In Ref. [16] we used the estimator

$$S = \frac{A_{c\max} - A_{c\min}}{A_{l\max} - A_{l\min}}, \tag{63}$$

where $A_{c\max}$ and $A_{c\min}$ are respectively the maximum and minimum amplitude of the function in the steep center region, and $A_{l\max}$ and $A_{l\min}$ are respectively the maximum and minimum of the flat lobes of Fig. 1. This estimator has many nice features, including its simplicity as well as resemblance to balanced detection [36]. It is also linear in the parameter for much of the subwavelength- resolved region. Nevertheless, the MaxLike estimator in Sec. III A is provably optimal. This is because the MaxLike estimator incorporates the sensitivity of changes of the function across the entire function. Nevertheless, the MaxLike estimator is nonlinear, and the simpler estimator above may be more practical. Nevertheless, we can quantify the advantages in precision the MaxLike estimator can provide. Furthermore, given a known model or range of models, MaxLike can be generalized to cases where the simplifying assumptions of our two- point scattering model break down.

The function $f(x)$ is used to compute the range resolution Fisher information in the field-detection case (which is proportional to the Fisher information in the photon-counting case, $I_p = 4\Sigma^2 I_f$). The scaled Fisher information $\Sigma^2 I_f$ is plotted in Fig. 2 as a function of $r = l\Omega/2\pi$. It vanishes as $l \to 0$ and behaves quadratically. The quadratic approximation, Eq. (11), is also plotted as I_{quad}, calculating

FIG. 3. The inner product between the original function and its reflected version [Eq. (25)] is plotted as a function of range separation l, in units of $2\pi/\Omega$. The overlap decays slowly as the fourth power of the separation [Eq. (29)], with the exact calculation shown in blue dots and the quartic approximation shown in black dashes. The triangle function overlap, with matched derivative at the origin, is plotted in solid red. The triangle overlap decays more quickly, indicating better resolvability, owing to its sharp cusps.

only the variance of the second derivative of the function $f(x)$, showing excellent agreement for small values of l that are subresolved.

The triangle function is nonanalytic, so a Fisher information analysis is not suitable. Nevertheless, we can compute the overlap metric in this case, and compare it to the band-limited function's behavior. The plot of the overlap metric [Eq. (25)] is shown as a function of the l parameter in Fig. 3 as a solid red curve. Compared to the band-limited function discussed in this section (plotted in dotted blue), its nonanalytic behavior leads to greater resolvability. This is because as soon as there is any separation, the interfered function cuts the top off the triangle, leading to flat regions. The drawback of this function is that it is no longer band-limited, and indeed contains high- frequency content [16]. In practice the cusp of the triangle will be slightly smoothed.

VI. MULTIPARAMETER ESTIMATION

In the sections above we focused on single-parameter estimation to set fundamental bounds on this technique. However, the real power behind super-radar will be to engage in many-parameter estimation for a variety of real-world sensing tasks. Therefore, we give a brief treatment here of the fundamental limits of multiparameter estimation, even if simpler estimation techniques are ultimately more practical.

We define a collection of parameters $\theta_1, \theta_2, \ldots, \theta_p$ that we wish to estimate. We focus on the field-detection measurements here, so the detected signal is $s(x_i) = \mathcal{N}_{\vec{\theta}} f_{\vec{\theta}}(x_i)$, plus detector noise, where the p parameters are encoded with a p-dimensional vector $\vec{\theta}$. The statistical model is
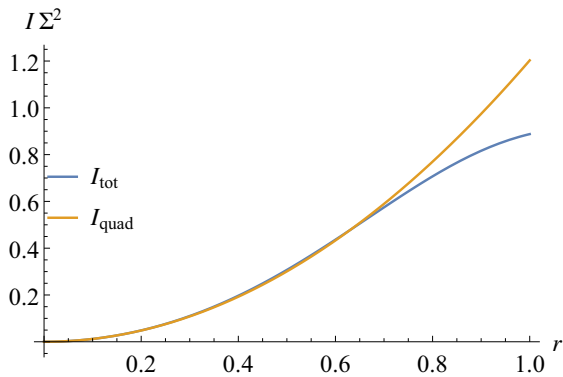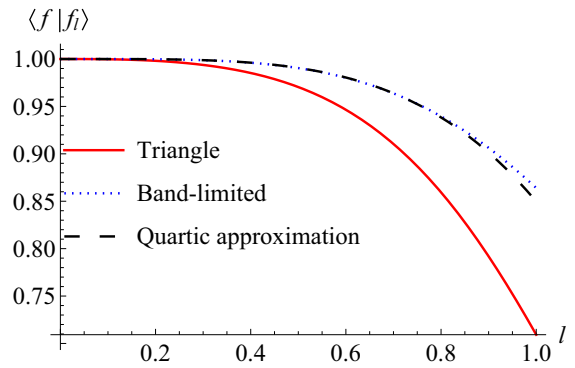

FIG. 2. Fisher information times noise strength is plotted versus target separation, in units of $2\pi/\Omega$, in the case of field detection. The entire parameter range shown is traditionally considered subresolved. The quadratic approximation I_{quad} is compared with the exact result $I_f = I_{\text{tot}}$.

then given by Eq. (5), where we replace the target range separation l with $\vec{\theta}$, the set of parameters imprinted on the scattered wave from the collection of targets, which can now be quite general. We define the single-repetition Fisher information matrix I_{jk} to be

$$I_{jk} = -\int \prod_i ds_i P(s_i|\vec{\theta}) \frac{\partial^2 \ln P(s_i|\vec{\theta})}{\partial\theta_j \partial\theta_k}. \qquad (64)$$

This matrix sets a bound on the covariance matrix of the parameters, $\mathrm{cov}[\theta_j\theta_k] = \langle\theta_j\theta_k\rangle - \langle\theta_j\rangle\langle\theta_k\rangle$, given by

$$\mathrm{cov}[\theta_j\theta_k] \geq (I^{-1})_{jk}, \qquad (65)$$

that generalizes the Cramér-Rao bound. Here I^{-1} is the matrix inverse of the Fisher information matrix. An expression for the Fisher information matrix can be derived as a generalization to Eq. (9). We find

$$
\begin{aligned}
I_{jk} &= \frac{1}{\Sigma^2}\int dx \frac{\partial(\mathcal{N}_{\vec{\theta}}f_{\vec{\theta}}(x))}{\partial\theta_j}\frac{\partial(\mathcal{N}_{\vec{\theta}}f_{\vec{\theta}}(x))}{\partial\theta_k}, \\
&= \frac{\mathcal{N}_{\vec{\theta}}^2}{\Sigma^2}\int dx \frac{\partial f_{\vec{\theta}}(x)}{\partial\theta_j}\frac{\partial f_{\vec{\theta}}(x)}{\partial\theta_k} - \frac{1}{\Sigma^2\mathcal{N}_{\vec{\theta}}^2}\frac{\partial\mathcal{N}_{\vec{\theta}}}{\partial\theta_j}\frac{\partial\mathcal{N}_{\vec{\theta}}}{\partial\theta_k},
\end{aligned} \quad (66)
$$

where we assume f is analytic, bounded, and square integrable. For M repetitions of the measurement, a factor of M appears as a prefactor to the Fisher information matrix. We note that optimal estimators saturating the matrix Cramér-Rao bound [Eq. (65)] are more difficult to find in the multiparameter case and may not exist in general.

A. Unequal weight reflectors

As a simple example of multiparameter estimation, we consider a slight generalization of the above two-point scatterer model, where the weights of the two reflections are unequal. In this case, the reflected function, Eq. (1), becomes

$$f_{l,p}(x) = pf(x - l/2) + (1 - p)f(x + l/2), \qquad (67)$$

where $p \in [0,1]$ is the relative weight of the two reflectors. In this case, the Fisher information matrix is 2×2, where $\vec{\theta} = (l,p)$. The function normalization $\mathcal{N}_{l,p}$ depends on both parameters in general. Defining the matrix $M_{jk} = \int dx\, \partial_{\theta_j} f_{\vec{\theta}}(x)\partial_{\theta_k} f_{\vec{\theta}}(x)$ that appears in Eq. (66) for convenience, we find the matrix elements of M to be

$$M_{ll} = \int dx \left(\frac{\partial f_{l,p}}{\partial l}\right)^2, \qquad (68)$$

where

$$\frac{\partial f_{l,p}}{\partial l} = \frac{1}{2}\left[-pf'(x - l/2) + (1 - p)f'(x + l/2)\right]. \quad (69)$$

The (p,p)th element is

$$M_{pp} = \int dx \left(\frac{\partial f_{l,p}}{\partial p}\right)^2 = \int dx(f(x - l/2) - f(x + l/2))^2. \qquad (70)$$

For small l, we have the approximation $M_{pp} \approx l^2 \int dx\, f'(x)^2$. The off-diagonal (l,p)th matrix element is given by

$$
\begin{aligned}
M_{lp} &= \int dx \frac{\partial f_{l,p}}{\partial l}\frac{\partial f_{l,p}}{\partial p} \\
&= (p - 1/2)\int dx\, f(x + l/2)f'(x - l/2). \qquad (71)
\end{aligned}
$$

The other off-diagonal matrix element $M_{pl} = M_{lp}$ by the equality of the mixed partial derivatives. We notice the discrete symmetry $p \to 1 - p$, $l \to -l$ both in the model and in the Fisher information matrix.

We focus on the most interesting case of deep subwavelength range resolution estimation, where we expand in l to leading order. We find the results

$$
\begin{aligned}
M_{ll} &\approx \left(\frac{1}{2} - p\right)^2 \int dx\, f'(x)^2 + \left(\frac{l}{4}\right)^2 \int dx\, f''(x)^2, \\
M_{pp} &\approx l^2 \int dx\, f'(x)^2, \\
M_{lp} &\approx \left(p - \frac{1}{2}\right) l \int dx\, f'(x)^2.
\end{aligned} \quad (72)
$$

We notice that if the reflectors are unbalanced, the first term in M_{ll} can be much larger than the second term, because the integral of the squared second derivative can be much smaller than the integral of the squared first derivative, because we have taken l to be much smaller than the characteristic size of the pulse. Thus, the case we have primarily focused on of perfectly balanced reflectors is the most challenging case for estimating range resolution. Adopting the unbalanced case, we find the contribution from the normalization is of subleading order, and can approximate

$$\Sigma^2 I \approx \int dx\, f'(x)^2 \begin{pmatrix} \left(\frac{1}{2} - p\right)^2 & \left(p - \frac{1}{2}\right)l \\ \left(p - \frac{1}{2}\right)l & l^2 \end{pmatrix}, \qquad (73)$$

where the basis choice is $\vec{\theta} = (l,p)$. Thus, the estimation uncertainties are dependent on each other. Indeed, in this special limit, we observe that the Fisher information matrix has a zero eigenvalue, indicating the model is singular in this limit. In hindsight, it is clear where the singularity comes from: the zero eigenvalue originates from

expanding our returning pulse Eq. (67) to leading order in l, p, $f_{lp}(x) \approx f(x) + (1/2 - p)lf'(x)$. We see the product of parameters $(1/2 - p)l$ appears at this order, indicating it is not possible to estimate each independently. We can break the singularity by keeping the order l^2 in the (l, l)th term of the Fisher information matrix,

$$\Sigma^2 I_{ll} \approx \left(\frac{1}{2} - p\right)^2 \int dx f'(x)^2 + \left(\frac{l}{4}\right)^2 \int dx f''(x)^2$$
$$- l^2(p^2 - p)^2 \left(\int dx f'(x)^2\right)^2, \tag{74}$$

which reproduces Eq. (11) when $p = 1/2$.

VII. CONCLUSIONS

We have explored the fundamental limits of remote sensing range resolution that is subwavelength, "super-radar." By applying the formal methods of parameter estimation as applied to known waveforms reflected off two point targets with equal amplitude reflections (for simplicity), we quantified the smallest resolvable distance between the two targets and bounded the precision of range resolution as a function of separation. We found general expressions for the Fisher information, which bounds the variance of the parameter of interest. As the separation of the targets goes to zero, the information vanishes quadratically with a prefactor proportional to the variance of the second derivative, evaluated in the waveform. We discussed different estimation methods, including Bayesian estimation and the optimal (nonlinear) maximum likelihood estimator, as well as a simpler balanced detection-type estimation method, which is linear for sufficiently large separation. We also considered photon detection and derived both Fisher information for space-resolved (or time-resolved) detection as well as the QFI, optimized to any measurement basis. We find similar results there to the field detection: the information also vanishes quadratically as separation decreases, and the results are equivalent up to a constant of proportionality. Nevertheless, these methods beat the traditional range resolution limits by orders of magnitude. We explored different bandlimited waveforms that can be implemented in super-radar, optimizing the variance of the second derivative that will be continued in future work. We also discussed multiparameter estimation, and set fundamental bounds on that task as well. In future work, we will implement these optimal estimators experimentally and demonstrate improved range resolution precision.

ACKNOWLEDGMENTS

[1] Naval Air Warfare Center, *Electronic Warfare and Radar Systems Engineering Handbook* (Electronic Warfare Division, Pont Mugu, CA, 1997).

[2] Richard J. Doviak and Dušan S. Zrnic, *Doppler Radar and Weather Observations* (Academic Press, Inc., San Diego, CA, 2006).

[3] Wen-Qin Wang, Overview of frequency diverse array in radar and navigation applications, IET Radar Sonar Navig. **10**, 1001 (2016).

[4] Rony Komissarov, Vitali Kozlov, Dmitry Filonov, and Pavel Ginzburg, Partially coherent radar unties range resolution from bandwidth limitations, Nat. Commun. **10**, 1423 (2019).

[5] Jan Francke, A review of selected ground penetrating radar applications to mineral resource evaluations, J. Appl. Geophys. **81**, 29 (2012).

[6] Adrian Neal, Ground-penetrating radar and its use in sedimentology: Principles, problems and progress, Earth-Sci. Rev. **66**, 261 (2004).

[7] Changzhi Li, Zhengyu Peng, Tien-Yu Huang, Teng-long Fan, Fu-Kang Wang, Tzyy-Sheng Horng, Jose-Maria Munoz-Ferreras, Roberto Gomez-Garcia, Lixin Ran, and Jenshan Lin, A review on recent progress of portable short-range noncontact microwave radar systems, IEEE Trans. Microw. Theory Tech. **65**, 1692 (2017).

[8] Pinliang Dong and Qi Chen, *LiDAR Remote Sensing and Applications* (CRC Press, Boca Raton, FL, 2017).

[9] Nadav Levanon and Eli Mozeson, *Radar Signals* (John Wiley & Sons, Hoboken, New Jersey, 2004).

[10] Merrill Ivan Skolnik, Introduction to radar systems (McGraw Hill Book Co., New York, 1980).

[11] Benjamin Nuss, Jonathan Mayer, Sören Marahrens, and Thomas Zwick, Frequency comb OFDM radar system with high range resolution and low sampling rate, IEEE Trans. Microw. Theory Tech. **68**, 3861 (2020).

[12] Behnam Behroozpour, Phillip A. M. Sandborn, Ming C. Wu, and Bernhard E. Boser, Lidar system architectures and circuits, IEEE Commun. Mag. **55**, 135 (2017).

[13] Emily D. Caldwell, Laura C. Sinclair, Nathan R. Newbury, and Jean-Daniel Deschenes, The time-programmable frequency comb and its use in quantum-limited ranging, Nature **610**, 667 (2022).

[14] Robert E. Sheriff, in *Seismic Stratigraphy—Applications to Hydrocarbon Exploration* (American Association of Petroleum Geologists, Boston, MA, 1977).

[15] Yiyu Zhou, Jing Yang, Jeremy D. Hassett, Seyed Mohammad Hashemi Rafsanjani, Mohammad Mirhosseini, A. Nick Vamivakas, Andrew N. Jordan, Zhimin Shi, and Robert W. Boyd, Quantum-limited estimation of the axial separation of two incoherent point sources, Optica **6**, 534 (2019).

[16] John C. Howell, Andrew N. Jordan, Barbara Šoda, and Achim Kempf, Super interferometric range resolution, Phys. Rev. Lett. **131**, 053803 (2023).

[17] Mankei Tsang, Quantum imaging beyond the diffraction limit by optical centroid measurements, Phys. Rev. Lett. **102**, 253601 (2009).

[18] Mankei Tsang, Subdiffraction incoherent optical imaging via spatial-mode demultiplexing, New J. Phys. **19**, 023054 (2017).

[19] Sultan Abdul Wadood, Kevin Liang, Yiyu Zhou, Jing Yang, M. A. Alonso, X-F Qian, Tanya Malhotra, S. M. Hashemi Rafsanjani, Andrew N. Jordan, and Robert W. Boyd, *et al.*, Experimental demonstration of superresolution of partially coherent light sources using parity sorting, Opt. Express **29,** 22034 (2021).

[20] Katherine K. M. Bearne, Yiyu Zhou, Boris Braverman, Jing Yang, S. A. Wadood, Andrew N. Jordan, A. N. Vamivakas, Zhimin Shi, and Robert W. Boyd, Confocal super-resolution microscopy based on a spatial mode sorter, Opt. Express **29,** 11784 (2021).

[21] Jing Yang, Shengshi Pang, Yiyu Zhou, and Andrew N. Jordan, Optimal measurements for quantum multiparameter estimation with general states, Phys. Rev. A **100,** 032104 (2019).

[22] Luo Qi, Xiaojie Tan, Lianwei Chen, Kenneth Y. W. Ng, Aaron J. Danner, and Mankei Tsang, in *CLEO: QELS_Fundamental Science* (Optica Publishing Group, San Jose, CA, 2022), p. JTu3A–22.

[23] Gregory E. Johnson, Edward R. Dowski, and W. Thomas Cathey, Passive ranging through wave-front coding: Information and application, Appl. Opt. **39,** 1700 (2000).

[24] Sean Quirin and Rafael Piestun, Depth estimation and image recovery using broadband, incoherent illumination with engineered point spread functions, Appl. Opt. **52,** A367 (2013).

[25] Aleksey N. Simonov, Cramer–Rao bounds in functional form: Theory and application to passive optical ranging, JOSA A **31,** 2680 (2014).

[26] Ronald Aylmer Fisher, Theory of statistical estimation, Math. Proc. Cambridge Philos. Soc. **22,** 700 (1925).

[27] Harald Cramér, *Mathematical Methods of Statistics* (Princeton University Press, Princeton, NJ, Princeton, NJ, 1999), Vol. 43.

[28] Andrew N. Jordan, Julián Martínez-Rincón, and John C. Howell, Technical advantages for weak-value amplification: When less is more, Phys. Rev. X **4,** 011031 (2014).2160-3308

[29] Steven M. Kay, *Fundamentals of Statistical Signal Processing: Estimation Theory* (Prentice-Hall, Inc., Upper Saddle River, NJ, 1993).

[30] Alexander Ly, Maarten Marsman, Josine Verhagen, Raoul PPP Grasman, and Eric-Jan Wagenmakers, A tutorial on Fisher information, J. Math. Psychol. **80,** 40 (2017).

[31] Andrew N. Jordan, Jeff Tollaksen, James E. Troupe, Justin Dressel, and Yakir Aharonov, Heisenberg scaling with weak measurement: A quantum state discrimination point of view, Quantum Stud.: Math. Found. **2,** 5 (2015).

[32] Carl W. Helstrom, Quantum detection and estimation theory, J. Stat. Phys. **1,** 231 (1969).

[33] Samuel L. Braunstein and Carlton M. Caves, Statistical distance and the geometry of quantum states, Phys. Rev. Lett. **72,** 3439 (1994).

[34] Barbara Šoda and Achim Kempf, Efficient method to create superoscillations with generic target behavior, Quantum Stud.: Math. Found. **7,** 347 (2020).

[35] Tathagata Karmakar and Andrew N. Jordan, Beyond superoscillation: General theory of approximation with bandlimited functions, Preprint ArXiv:2306.03963 (2023).

[36] P. Ben Dixon, David J. Starling, Andrew N. Jordan, and John C. Howell, Ultrasensitive beam deflection measurement via interferometric weak value amplification, Phys. Rev. Lett. **102,** 173601 (2009).